Ligand Dehydrogenation in Ruthenium−Amine Complexes: Reactivity of 1,2-Ethanediamine and 1,1,1-Tris(aminomethyl)ethane†

Paul Bernhard,*[,1a] Daryl J. Bull,*[,1b] Hans-Beat Bürgi,*[,‡,1c] Peter Osvath,*[,§,1b,d] Andrea Raselli,*[,1c] and Alan M. Sargeson*[,∥,1b]

Research School of Chemistry, Australian National University, Canberra, ACT 0200, Australia, Laboratorium für Chemische und Mineralogische Kristallographie, Universität Bern, CH-3012 Bern, Switzerland, and Ciba-Geigy AG, CH-1701 Fribourg, Switzerland

Received August 22, 1996[⊗]

The mechanisms of oxidative ligand dehydrogenation in high-valent ruthenium hexaamine complexes of bidentate 1,2-ethanediamine (en) and tridentate 1,1,1-tris(aminomethyl)ethane (tame) are elucidated in detail. In basic aqueous solution, $[Ru^{III}(tame)_2]^{3+}$ undergoes rapid initial deprotonation ($pK_{III} = 10.3$). This is followed by a pH-dependent disproportionation step involving either $[Ru^{III}(tame)_2\text{-}H^+]^{2+} + [Ru^{III}(tame)_2]^{3+}$ ($k_{1d} = 8300\ M^{-1}\ s^{-1}$) or two singly deprotonated $[Ru^{III}(tame)_2\text{-}H^+]^{2+}$ ions ($k_{2d} = 3900\ M^{-1}\ s^{-1}$). The products are $[Ru^{II}(tame)_2]^{2+}$ and either the singly deprotonated species $[Ru^{IV}(tame)_2\text{-}H^+]^{3+}$ ($pK_{IV} = 8.2$) or the doubly deprotonated $[Ru^{IV}(tame)_2\text{-}2H^+]^{2+}$. These Ru(IV) complexes undergo spontaneous dehydrogenation to give the imine $[Ru^{II}(imtame)(tame)]^{2+}$ (imtame = 1,1-bis(aminomethyl)-1-(iminomethyl)ethane), with first-order rate constants of $k_{1im} = 320\ s^{-1}$ and $k_{2im} = 1.1\ s^{-1}$, respectively. In the $[Ru^{III}(en)_3]^{3+}$ system, the initial deprotonation ($pK_{III} = 10.4$) is followed by the corresponding disproportionation reactions ($k_{1d} = 9000\ M^{-1}\ s^{-1}$, $k_{2d} = 3800\ M^{-1}\ s^{-1}$). The complex $[Ru^{IV}(en)_3\text{-}H^+]^{3+}$ ($pK_{IV} = 8.9$) and its deprotonated counterpart, $[Ru^{IV}(en)_3\text{-}2H^+]^{2+}$, undergo dehydrogenation to give $[Ru^{II}(imen)(en)_2]^{2+}$ (imen = 2-aminoethanimine) with first-order rate constants of $k_{1im} = 600\ s^{-1}$ and $k_{2im} = 1.0\ s^{-1}$, respectively. In the light of this analysis, the disproportionation and ligand oxidation of the $[Ru^{III}(sar)]^{3+}$ ion are reexamined ($k_{1d} = 4 \times 10^7\ M^{-1}\ s^{-1}$, $k_{2d} \geq 2 \times 10^7\ M^{-1}\ s^{-1}$, $pK_{IV} = 2.0$, $k_{1im} = 17\ s^{-1}$, $k_{2im} = 5 \times 10^{-4}\ s^{-1}$ at 25 °C). While the disproportionation to Ru(II) and Ru(IV) has been recognized in such systems, the complexity of the paths has not been realized previously; the surprising variation in the rates of the intramolecular redox reaction (from days to milliseconds) is now dissected and understood. Other facets of the intramolecular redox reaction are also analyzed.

Introduction

A number of transition metal ions in high oxidation states have the ability to oxidize coordinated amines to coordinated imines. Examples of such intramolecular oxidations have been reported to occur with iron,[2,3] copper,[4] nickel,[5−9] ruthenium,[10−23] osmium,[24−27] and platinum.[28] In related reactions, coordinated alcohols are oxidized to aldehydes or ketones.[29,30] Intermolecular oxidations by high oxidation state metal compounds have also been reported. For example, $[(trpy)(bpy)Ru{=}O]^{2+}$ (trpy = 2,2′,2″-terpyridine; bpy = 2,2′-bipyridine) can be used to oxidize $(CH_3)_2CHOH$ to $(CH_3)_2C{=}O$.[31] Such examples highlight the potential of transition metals in high oxidation states for efficient and controlled two-electron oxidations in organic synthesis.

† Dedicated to Professor Wolfgang Beck, friend, scholar, and gentleman.

‡ E-mail: hbuergi@krist.unibe.ch.
§ E-mail: p.osvath@chem.csiro.au.
∥ E-mail: sargeson@rsc.anu.edu.au.

⊗ Abstract published in *Advance ACS Abstracts,* May 1, 1997.

(1) (a) Ciba-Geigy. (b) Australian National University. (c) Universität Bern. (d) Current address: CSIRO Division of Chemicals and Polymers, Private Bag 10, Clayton South MDC, Clayton, VIC 3169, Australia.
(2) Goto, M.; Takeshita, M.; Kanda, N.; Sakai, T.; Goedken, V. L. *Inorg. Chem.* **1985**, *24*, 582.
(3) Goedken, V. L. *J. Chem. Soc., Chem. Commun.* **1972**, 207.
(4) Olson, D. C.; Vasilevskis, J. *Inorg. Chem.* **1971**, *10*, 463.
(5) Barefield, E. K.; Mocella, M. T. *J. Am. Chem. Soc.* **1975**, *97*, 4238.
(6) Morliere, P.; Patterson, L. K. *Inorg. Chem.* **1982**, *21*, 1833.
(7) Maruthamuthu, P.; Patterson, L. K.; Ferraudi, G. *Inorg. Chem.* **1978**, *17*, 3157.
(8) Jaacobi, M.; Meyerstein, D.; Lilie, J. *Inorg. Chem.* **1979**, *18*, 429.
(9) Curtis, N. F. *J. Chem. Soc. A* **1971**, 2834.
(10) Lane, B. C.; Lester, J. E.; Basolo, F. *J. Chem. Soc., Chem. Commun.* **1971**, 1618.
(11) McWhinnie, W. R.; Miller, J. D.; Watts, J. B.; Wadden, D. Y. *J. Chem. Soc., Chem. Commun.* **1971**, 629.
(12) Mahoney, D. F.; Beattie, J. K. *Inorg. Chem.* **1973**, *12*, 2561.
(13) Diamond, S. E.; Tom, G. M.; Taube, H. *J. Am. Chem. Soc.* **1975**, *97*, 2661.
(14) Wong, K.-Y.; Che, C.-M.; Li, C.-K.; Chiu, W.-H.; Zhou, Z.-Y.; Mak, T. C. W. *J. Chem. Soc., Chem. Commun.* **1992**, 754.
(15) Ridd, M. J.; Keene, F. R. *J. Am. Chem. Soc.* **1981**, *103*, 5733.
(16) Keene, F. R.; Ridd, M. J.; Snow, M. R. *J. Am. Chem. Soc.* **1983**, *105*, 7075.
(17) Adcock, P. A.; Keene, F. R.; Smythe, R. E.; Snow, M. R. *Inorg. Chem.* **1984**, *23*, 2336.
(18) Whebell, G. W.; Keene, F. R. *Aust. J. Chem.* **1986**, *39*, 2027.
(19) Alvarez, V. E.; Allen, R. J.; Matsubara, T.; Ford, P. C. *J. Am. Chem. Soc.* **1974**, *96*, 7686.
(20) Miller, J. D.; Watts, J. B.; Waddan, D. Y. *Inorg. Chim. Acta* **1975**, *12*, 267.
(21) Brown, G. M.; Weaver, T. R.; Keene, F. R.; Meyer, T. J. *Inorg. Chem.* **1976**, *15*, 190.
(22) Keene, F. R.; Salmon, D. J.; Meyer, T. J. *J. Am. Chem. Soc.* **1976**, *98*, 1884.
(23) Hoshino, Y.; Okuyama, F.; Nanba, A.; Shimizu, K.; Sato, G. P. *Bull. Chem. Soc. Jpn.* **1992**, *65*, 876.
(24) Lay, P. A. Ph.D. Thesis, Australian National University, 1981.
(25) Lay, P. A.; Sargeson, A. M.; Skelton, B. W.; White, A. H. *J. Am. Chem. Soc.* **1982**, *104*, 6161.
(26) Lay, P. A.; Sargeson, A. M. *Inorg. Chim. Acta* **1992**, *198−200*, 449.
(27) Keene, F. R.; Lay, P. A.; Sneddon, G. E.; Whebell, G. W. *Aust. J. Chem.* **1993**, *46*, 1763.
(28) Schwarz, F.; Schöllhorn, H.; Thewalt, U.; Lippert, B. *J. Chem. Soc. Chem. Commun.* **1990**, 1282.
(29) Tovrog, B. S.; Diamond, S. E.; Mares, F. *J. Am. Chem. Soc.* **1979**, *101*, 5067.
(30) Ridd, M. J.; Gakowski, D. J.; Sneddon, G. E.; Keene, F. R. *J. Chem. Soc., Dalton Trans.* **1992**, 1949.
(31) Thompson, M. S.; Meyer, T. J. *J. Am. Chem. Soc.* **1982**, *104*, 4106.

S0020-1669(96)01021-X CCC: $14.00

Scheme 1

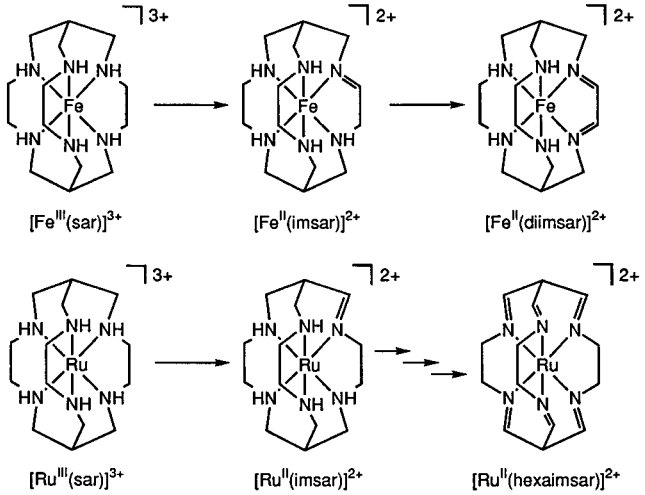

Scheme 2

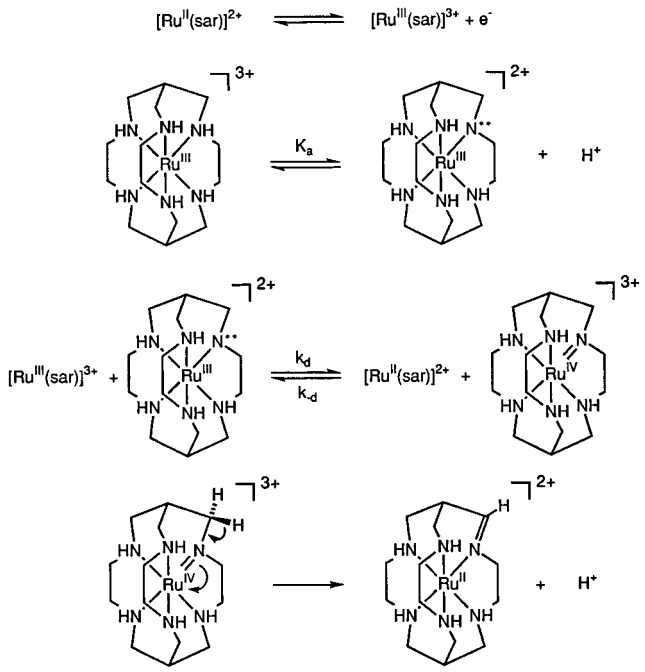

The current work was prompted by the observation of related ligand dehydrogenations which occur with cage complexes such as $[Fe^{III}(sar)]^{3+}$ and $[Ru^{III}(sar)]^{3+}$ (sar = 3,6,10,13,16,19-hexaazabicyclo[6.6.6]icosane). The oxidation generates imines in the coordinated ligands in a regioselective manner (Scheme 1).[32,33] In the iron complex, the imine forms in the five-membered chelate ring of the cage,[32] whereas in the ruthenium complex, the imine forms in the cap of the cage.[33] Both molecules can be oxidized further, in the case of iron to a diimine complex and in the case of ruthenium to a hexaimine complex. For both metals, the regiospecificity is retained in the subsequent oxidation steps.

A previous detailed study of the $[Ru^{III}(sar)]^{3+}$ system[33] led to a proposal for the mechanism of oxidation to the monoimine (Scheme 2). This involved a disproportionation step, in which electron transfer took place from a singly deprotonated Ru(III)−amine complex to a fully protonated Ru(III)−amine complex. It gave rise to a Ru(II)−amine complex and a deprotonated Ru(IV)−amine complex in which there was increased bond order between the metal and the deprotonated nitrogen. The rate constant for the disproportionation was calculated as $(6-9) \times 10^7$ M^{-1} s^{-1}, and the rate constant for the comproportionation, as 6.2×10^3 M^{-1} s^{-1}. The deprotonated Ru(IV)−amine complex then decayed by an irreversible intramolecular redox reaction to a Ru(II)−imine complex. This was the first direct observation of such a Ru(IV) intermediate. This intermediate could also be generated quantitatively under suitable conditions, and its first-order decay to the Ru(II)−imine complex could then be observed separately. While some mechanistic detail was unraveled in that paper,[33] the reasons for the rapid oxidation relative to other Ru(III)−amine complexes were not evident, especially since the Ru(III)/Ru(II) reduction potential was not high.

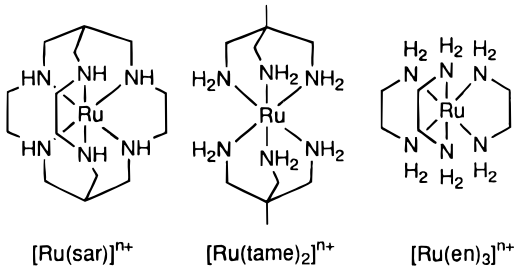

Figure 1. Ruthenium complexes.

The ligand oxidation of $[Ru^{III}(sar)]^{3+}$ is unusual since this reaction is very rapid even in strongly acidic solutions.[33] For example, the imine formation occurs in less than 1 s at pH 2.3. This behavior is in contrast to that of other Ru(III)-saturated amine complexes which are usually stable under acidic conditions.[10−23,34] The unusually high reactivity and the regioselectivity for the dehydrogenation of $[Ru^{III}(sar)]^{3+}$ are intriguing. To examine this problem in detail, the Ru(III) complexes of the ligands 1,1,1-tris(aminomethyl)ethane (tame) and 1,2-ethanediamine (en) were investigated, since they represent two different fragments of the cage complex: the bis(tame) complex models the "cap" fragments whereas the tris(en) complex models the "body" of [Ru(sar)] (Figure 1).

Experimental Section

Materials. Doubly deionized Milli-Q reagent water was used for kinetic experiments. Commercially available argon was passed over molecular sieves and a BASF catalyst to remove traces of water and O_2 prior to use. Ruthenium powder was obtained from Platinum Chemicals. Sodium hydroxide solutions were purchased as carbonate-free volumetric solutions and stored under N_2. Other reagents were of analytical grade and were used without further purification.

Physical Measurements. Absorption spectra were recorded with HP 8450 and Cary 118 spectrophotometers. The solutions used for recording the absorption spectra were prepared by dissolving a known amount of the complex in a known volume of the appropriate solvent which had been flushed with argon for at least 20 min. For the Ru(II) solutions, a piece of amalgamated zinc was added during the argon-bubbling procedure. The solutions were flushed with argon for 20 min, and the spectra were then recorded.

For kinetic experiments with the HP 8450 and Cary 118 spectrophotometers, a thermostated mixing device was used (mixing time ~0.5 s). Fast kinetic experiments ($t_{1/2}$ < 10 s) were performed with an Applied Photophysics SF 17 MV stopped-flow spectrophotometer. The formation or decay of the different Ru−amine species could be monitored by the appropriate choice of wavelength.

The oxidants used to generate the Ru(IV) oxidation state directly were O_2, $[Fe(CN)_6]^{3-}$, and $[Os(CN)_6]^{3-}$. Due to the O_2 sensitivity of some of the reactions, the following steps were taken to exclude adventitious air from the reaction mixtures. All solutions were saturated with argon for 20 min prior to use, and the experiments were carried

(32) Hagen, K. S.; Sargeson, A. M. Unpublished.
(33) Bernhard, P.; Sargeson, A. M. *J. Am. Chem. Soc.* **1989**, *111*, 597.
(34) Smolenaers, P. J. Ph.D. Thesis, University of Sydney, 1981.

out as quickly as possible. The sample-handling unit of the stopped-flow spectrophotometer and the hand mixer were enclosed within glovebags containing a nitrogen atmosphere. As a precaution against O_2 absorbed in the Teflon flow lines of the stopped-flow sample-handling unit, the reagent reservoirs, drive syringes, stopping syringes, and flow lines were soaked overnight with a sodium dithionite solution (5×10^{-3} M buffered at pH 8.0). The equipment was then washed thoroughly with argon-saturated deionized water. The circulating solution in the thermostat bath also contained Tris/HCl buffer (pH ~8), and nitrogen was continuously bubbled into this solution. Sodium dithionite (1 g) was added to this buffer at regular intervals to ensure that the system remained O_2 free.

The two solutions used for the kinetic experiments were prepared as follows. For the first solution, a known volume of 10^{-3} M $HClO_4$ was flushed with water-saturated argon for 20 min prior to addition of a known amount of the metal(III)−amine salt. The other solution was prepared similarly by flushing a standard NaOH solution or a buffered solution with water-saturated argon for 20 min and then adding a known amount of oxidant when required. Finally, both solutions were transferred under N_2 to the reservoir chambers of the stopped-flow unit or hand mixer. All experiments were performed at 25.0 ± 0.2 °C. Unless otherwise indicated, solutions were adjusted to 0.10 M ionic strength with $NaClO_4$.

All reactions were followed for at least 3 half-lives with an average of three experiments performed per set of reaction conditions. With these precautions, the observed rates were reproducible to within 10%. Absorbance−time curves were fitted to the following first- or second-order equation:

$$A_t = A_\infty + (A_0 - A_\infty)\exp(-k_{obs}t)$$

$$A_t = A_\infty + (A_0 - A_\infty)/(1 + k_{obs}t)$$

The buffers used in the kinetic experiments were guanidine hydrochloride/LiOH (pH 11.7−12.5), piperidine/HCl (pH 10.6−11.2), 3-(cyclohexylamino)propanesulfonic acid/LiOH (pH 10.3−10.6), piperazine/HCl (pH 9.5−10.1), 2-(cyclohexylamino)ethanesulfonic acid/LiOH (pH 9.2−9.5), diethanolamine/HCl (pH 8.5−8.9), tris(hydroxymethyl)aminomethane/HCl (pH 7.6−8.5), 4-(2-hydroxyethyl)-1-piperazineethanesulfonic acid/LiOH (pH 7.3−7.8), and 1,4-piperazinebis(ethanesulfonic acid)/LiOH (pH 6.6−7.1). All buffers were stored under nitrogen to prevent absorption of CO_2. The pH of each buffer was measured at 25.0 °C, with a Radiometer 26 pH meter, a G202D glass electrode, and a K401 calomel reference electrode. The pH meter was calibrated with a sodium/potassium phosphate buffer (pH 7.00) and a potassium phosphate/sodium borate buffer (pH 9.00). All measurements were conducted under a blanket of nitrogen.

The absorption spectra of short-lived species such as $[Ru^{III}(tame)_2\text{-}H^+]^{2+}$ and $[Ru^{IV}(tame)_2\text{-}2H^+]^{2+}$ [35] were obtained with the stopped-flow spectrophotometer. A series of experiments were carried out in which a slightly acidic solution of the metal−amine complex was mixed with a NaOH solution in the stopped-flow spectrophotometer, and the absorbance of this solution was recorded for 0.1 s. The absorbance reading was extrapolated to zero time (~1 ms). The measurement was repeated at a number of wavelengths from 350 to 700 nm, and the absorbance values at zero time were used to generate the point-by-point spectrum.

The acidity constants of the Ru(III) amines were determined spectrophotometrically using the stopped-flow spectrophotometer. Two solutions were prepared in the same manner as those used for the kinetic experiments. The wavelength was set to the λ_{max} of the deprotonated species of interest. (The fully protonated forms of these complexes have negligible absorbance at these wavelengths.) At each pH, the absorbance was recorded for 0.1 s and extrapolated to zero time. After a preliminary determination of the pK_a, a series of buffers (each 0.02 M) were prepared and the determinations were repeated at pH values equal to the preliminary value of the pK_a and at pK_a ± 0.2, ± 0.4, and ± 0.6. Other buffers outside this range were used to confirm that on either side of the pK_a the absorbance of the complexes reached an upper and a lower limiting value. The final pK_a values were then calculated by a standard method.[36]

^{1}H and proton-decoupled ^{13}C NMR spectra were recorded with either a Varian XL 200E or a Varian VXR 300 spectrometer. Chemical shifts in D_2O (δ, positive downfield) are given relative to 3-(trimethylsilyl)-propanesulfonate (0.00 ppm ^{1}H) and tetramethylsilane (0.00 ppm ^{13}C), using a value of 67.4 ppm for the ^{13}C signal of 1,4-dioxane as the internal reference.

Data Manipulation. Kinetic calculations were performed on either a Macintosh IIfx or a Vax 11/750 computer. The following programs were used: EXPFIT, which is a least-squares program for calculating rate constants in consecutive first-order reactions;[37] REACTION KINETICS, which uses a Runge-Kutta solution to simulate data for a second-order reaction followed by a first-order reaction where the half-lives for both reactions are similar (Written by D. J. Evans; see Supporting Information); IGOR[38] or KaleidaGraph,[39] for least-squares calculations to determine pK_a values and the pH dependence profiles of the measured rate constants.

Syntheses. Standard Schlenk techniques,[40] using an atmosphere of purified argon, were used for the manipulation of air-sensitive solutions. All solvents used for air-sensitive work were saturated with argon immediately prior to use. All solutions of fixed concentration were purged with argon that was saturated with the appropriate solvent. $Na_3[Fe(CN)_6]\cdot 2H_2O$ was prepared by passing a solution of $K_3[Fe(CN)_6]$ through a Dowex 50W-X2 column in the Na^+ form. Anal. Calcd for $Na_3[Fe(CN)_6]\cdot 2H_2O$: C, 22.7; H, 1.3; N, 26.5; Fe, 17.6. Found: C, 22.9; H, 1.0; N, 26.2; Fe, 17.5; K, 0.0. $[(C_6H_5)_3CH_3As]_2K[Os(CN)_6]\cdot H_2O$ was prepared by stoichiometric oxidation of $K_4[Os(CN)_6]$ with $KMnO_4$ and subsequent addition of $[(C_6H_5)_3CH_3As]Cl$. Anal. Calcd for $[(C_6H_5)_3CH_3As]_2K[Os(CN)_6]\cdot H_2O$: C, 50.5; H, 3.7; N, 8.0. Found: C, 50.3; H, 4.0; N, 7.7. $[Ru^{II}(tame)_2](C_7H_8SO_3)_2$, $[Ru^{III}(tame)_2]Cl_2ClO_4$, $[Ru^{II}(en)_3][ZnCl_4]$, and $[Ru^{III}(en)_3][ZnCl_4]Cl$ were prepared as described elsewhere.[41]

(a) [1,1,1-Tris(aminomethyl)ethane][1,1-bis(aminomethyl)-1-(iminomethyl)ethane]ruthenium(II) Iodide, $[Ru^{II}(imtame)(tame)]I_2$. $Na_3[Fe(CN)_6]\cdot 2H_2O$ (12 mg, 0.044 mmol) was dissolved in a solution of argon-saturated NaOH (6 mL, 0.1 M). This solution was then added to an argon-saturated solution of $[Ru^{III}(tame)_2]Cl_2ClO_4$ (20 mg, 0.04 mmol) in water (2 mL). After 1 min, NaI (0.6 g) was added to the yellow solution, and the mixture was cooled to 5 °C overnight, during which a yellow complex precipitated. The complex was recovered by filtration, washed with cold ethanol (2 × 5 mL) and dried in vacuo overnight. Anal. Calcd for $[Ru(C_5H_{13}N_3)(C_5H_{15}N_3)]I_2$: C, 20.5; H, 4.8; N, 14.3; I, 47.6. Found: C, 20.6; H, 5.1; N, 13.9; I, 47.5. ^{1}H NMR $\delta(D_2O)$: 8.2 (s, 1H, CH); 2.7 (s, 2H, CH_2); 2.6 (s, 4H, CH_2); 2.3 (s, 4H, CH_2); 1.08 (s, 3H, CH_3); 0.63 (s, 3H, CH_3). ^{13}C NMR $\delta(D_2O)$: 180.8 (N=CH); 50.1 (CH_2); 49.8 (CH_2); 45.1 (CH_2); 44.5 (quaternary C); 39.2 (quaternary C); 23.4 (CH_3); 21.5 (CH_3).

(b) (2-Aminoethanimine)bis(1,2-ethanediamine)ruthenium(II) Iodide, $[Ru(imen)(en)_2]I_2$. $Na_3[Fe(CN)_6]\cdot 2H_2O$ (12 mg, 0.044 mmol) was dissolved in a solution of argon-saturated NaOH (6 mL, 0.1 M). This solution was then added to an argon-saturated solution of $[Ru(en)_3][ZnCl_4]Cl$ (20 mg, 0.038 mmol) in water (2 mL). After 1 min, NaI (0.6 g) was added to the yellow solution, and the mixture was cooled to 5 °C overnight, during which yellow needles appeared. The complex was collected, washed with cold ethanol (2 × 5 mL), and

(35) In this publication, the following notations will be used: $[M^{III}(amine)_x\text{-}H^+]^{2+}$ represents a metal(III)−amine complex which has been deprotonated once. $[M^{IV}(amine)_x\text{-}2H^+]^{2+}$ represents a metal(IV) amine which has been deprotonated twice. For $x = 1$, the ligand is hexadentate and it is likely that the second deprotonation is *cis* to the first, but not in the same en chelate ring if the parallel to the Os^{IV} chemistry holds.[24−26] For $x = 2$ or 3 (tridentate and bidentate ligands, respectively), it is likely that two ligands are each singly deprotonated in the same manner.

(36) Albert, A.; Serjeant, E. P. *The Determination of Ionization Constants*, 3rd ed.; Chapman and Hall: London, 1984.
(37) Osborne, M. R. In *Numerical Methods for Non-Linear Optimization*; Lootsma, F. A., Ed.; Academic Press: New York, 1972; Chapter 11.
(38) IGOR Version 1.26, Wavemetrics Inc.
(39) KaleidaGraph Version 3.0.1, Abelbeck Software.
(40) Shriver, D. F.; Drezdzon, M. A. *The Manipulation of Air Sensitive Compounds*; 2nd ed.; Wiley: New York, 1986.
(41) Bernhard, P.; Bull, D. J.; Bürgi, H. B.; Raselli, A.; Sargeson, A. M. In preparation.

Scheme 3

Overall reaction process:

$$2[Ru^{III}(amine)]^{3+} \longrightarrow [Ru^{II}(imine)]^{2+} + [Ru^{II}(amine)]^{2+} + 2H^+$$

$$[Ru^{III}(amine)]^{3+} \overset{K_{III}}{\rightleftharpoons} [Ru^{III}(amine)\text{-}H^+]^{2+} + H^+$$

$$[Ru^{III}(amine)]^{3+} + [Ru^{III}(amine)\text{-}H^+]^{2+} \xrightarrow{k_{1d}} [Ru^{II}(amine)]^{2+} + [Ru^{IV}(amine)\text{-}H^+]^{3+}$$

$$2\,[Ru^{III}(amine)\text{-}H^+]^{2+} \xrightarrow{k_{2d}} [Ru^{II}(amine)]^{2+} + [Ru^{IV}(amine)\text{-}2H^+]^{2+}$$

$$[Ru^{IV}(amine)\text{-}H^+]^{3+} \overset{K_{IV}}{\rightleftharpoons} [Ru^{IV}(amine)\text{-}2H^+]^{2+} + H^+$$

$$[Ru^{IV}(amine)\text{-}H^+]^{3+} \xrightarrow{k_{1im}} [Ru^{II}(imine)]^{2+} + H^+$$

$$[Ru^{IV}(amine)\text{-}2H^+]^{2+} \xrightarrow{k_{2im}} [Ru^{II}(imine)]^{2+}$$

dried in vacuo. Anal. Calcd for $[Ru(C_6H_{22}N_6)]I_2$: C, 13.5; H, 4.2; N, 15.7; I, 47.6. Found: C, 13.6; H, 4.2; N, 15.2; I, 48.1.

Results

Experimental investigations and their interpretation were guided by the mechanism outlined for $[Ru^{III}(sar)]^{3+}$ in the Introduction (Scheme 2) and generalized in Scheme 3. The overall reaction is a sequence of two separate processes: (i) the disproportionation of two Ru(III) species and (ii) intramolecular ligand oxidation/metal reduction. Both steps are complicated by the presence of acid−base equilibria for the reactants and by the observation of significant reactivities in both protonation states of the reactants. A further complication arises from the fact that, under the conditions accessible for the experiments, disproportionation and imine formation occur on similar time scales.

The puzzle has been unraveled in several steps as described in detail for the $[Ru^{III}(tame)_2]^{3+}$ complex: After spectroscopic characterization of the final product $[Ru^{II}(imtame)(tame)]^{2+}$, general evidence for a two-step mechanism is presented. For each of the two steps, one of the putative molecules is then characterized ($[Ru^{III}(tame)_2\text{-}H^+]^{2+}$ and $[Ru^{IV}(tame)_2\text{-}2H^+]^{2+}$). Kinetic results are then presented for the second step. These have been obtained by bypassing the first step (i.e., producing $[Ru^{IV}(tame)_2\text{-}2H^+]^{2+}$ by rapid oxidation, directly from $[Ru^{III}(tame)_2\text{-}H^+]^{2+}$ rather than through disproportionation). With this information it was finally possible to deconvolute the kinetics of the disproportionation step from the experiments and to arrive at the overall picture given in Scheme 3.

Spectroscopic Properties of $[Ru^{II}(imtame)(tame)]^{2+}$. The electronic absorption spectrum of the monoimine complex $[Ru^{II}(imtame)(tame)]^{2+}$ has a band with λ_{max} at 390 nm (ϵ 4150 M^{-1} cm^{-1}), which is presumably of metal to ligand charge transfer ($d \rightarrow \pi^*$) origin. This band corresponds closely with a band in the spectrum of $[Ru^{II}(imsar)]^{2+}$, λ_{max} at 390 nm (ϵ 4300 M^{-1} cm^{-1}).[33] Similarly, the monoimine complex $[Ru^{II}(imen)(en)_2]^{2+}$ has λ_{max} at 375 nm (ϵ 3800 M^{-1} cm^{-1}). The magnitudes of these molar absorption coefficients for the $t_{2g} \rightarrow \pi^*$ metal to ligand charge transfer transitions are consistent with values reported for other monoimine complexes.[10−23,33] The different values of ϵ_{max} reported[42,43] for the $[Ru^{II}(en)_3]^{2+}$ ion have been discussed elsewhere.[41] Here we emphasize that 2% of the monoimine species contaminating $[Ru^{II}(en)_3]^{2+}$ would contribute ~80 M^{-1} cm^{-1} to ϵ_{max} at 370 nm, and this impurity would thus account for the observed variation of ϵ_{max}. The diimine, $[Ru^{II}(diimen)(en)_2]^{2+}$, has λ_{max} at 448 nm (ϵ 7000 ± 200 M^{-1} cm^{-2}) in agreement with the literature values.[12,44] Moreover, the intensity of the corresponding absorption maximum in the diimine complex is roughly double that of the monoimine complex.

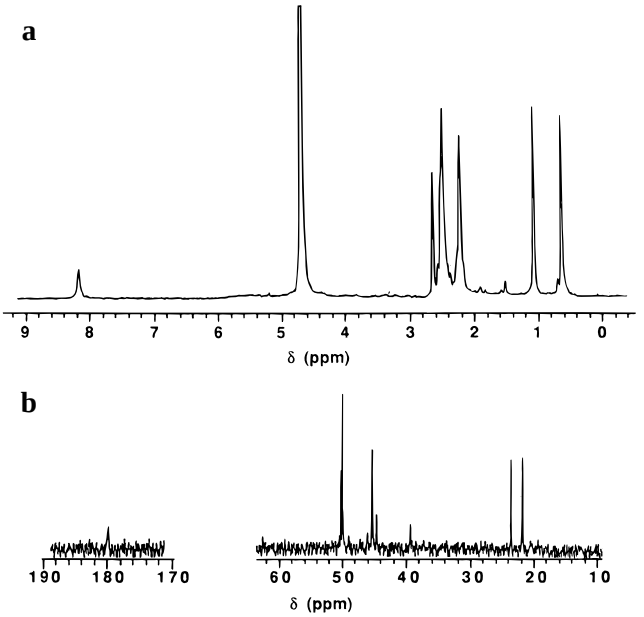

Figure 2. (a) 300 MHz ^1H and (b) 75 MHz ^{13}C NMR spectra of $[Ru^{II}(imtame)(tame)]^{2+}$ (HOD at ~4.7 ppm).

The ^1H and ^{13}C NMR spectra (Figure 2) are fully consistent with the structure of $[Ru^{II}(imtame)(tame)]^{2+}$ deuterated at the N centers. The peak positions and their integrals confirm that a single amine has been oxidized to the corresponding imine. Detailed assignment of the signals is described in the Supporting Information.

Reactivity of $[Ru^{III}(tame)_2]^{3+}$. When basic aqueous solutions of $[Ru^{III}(tame)_2]^{3+}$ were prepared, an intense yellow color quickly developed. The initial evidence that this reaction involved a disproportionation step was supplied by an NMR experiment. $[Ru^{III}(tame)_2]Cl_3$ was dissolved in 0.1 M NaOD, and well-resolved ^1H and ^{13}C NMR spectra could be recorded. The ^1H NMR spectrum was then recorded again after 15 min, and no change was observed in the spectrum. The ^1H NMR and ^{13}C NMR spectra of the reaction mixture showed the presence of two different diamagnetic compounds, namely $[Ru^{II}(tame)_2]^{2+}$ and $[Ru^{II}(imtame)(tame)]^{2+}$. The two compounds were in the ratio 1:1 as judged by the relative intensity of the ^1H NMR signals at 2.69 and 2.53 ppm, which correspond to the methylene protons in the oxidized and unoxidized ligands, respectively (see Supporting Information). This implied that $[Ru^{III}(tame)_2]^{3+}$ had disproportionated to give $[Ru^{II}(tame)_2]^{2+}$ and a Ru(IV) species which had then undergone a rapid intramolecular redox reaction to give $[Ru^{II}(imtame)(tame)]^{2+}$ in the basic medium (cf. Scheme 2).

The reaction was followed spectrophotometrically in more detail. The spectrum of a solution containing $[Ru^{III}(tame)_2]^{3+}$ (120 μM) and NaOH (4.5 mM) was recorded every 5 s. The spectra for the first 60 s are shown in Figure 3. It is clear that more than one reaction has occurred. The initial spectrum (a) has a maximum at 430 nm, where $[Ru^{IV}(tame)_2\text{-}2H^+]^{2+}$ is expected to absorb. The following spectrum (b) has a maximum at 390 nm, the wavelength at which $[Ru^{II}(imtame)(tame)]^{2+}$ is expected to absorb, but the bandwidth and shape also imply

(42) Meyer, T. J.; Taube, H. *Inorg. Chem.* **1968**, *7*, 2369.
(43) Elsbernd, H.; Beattie, J. K. *Inorg. Chem.* **1969**, *8*, 893.
(44) Elsbernd, H.; Beattie, J. K. *J. Chem. Soc. (A)* **1970**, 2598.

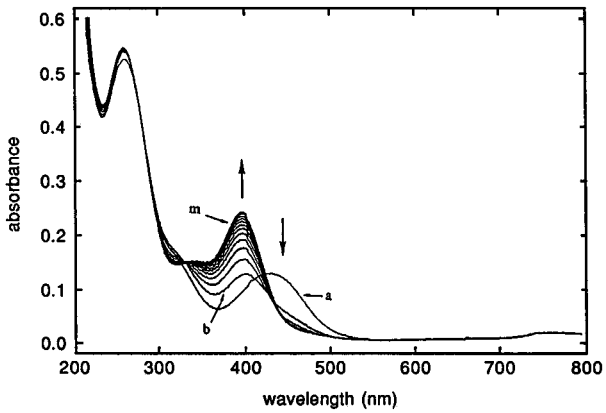

Figure 3. Absorption spectra of a reaction mixture containing $[Ru^{III}(tame)_2]^{3+}$ (120 μM) in OH^- solution (4.5 mM) recorded at 5 s intervals for the first 60 s of the reaction (25.0 °C, $I = 0.1$ M).

that at this point the reaction mixture contains species other than the monoimine.

The maximum molar absorption coefficient (ϵ_{max}) after this reaction was complete (Figure 3, m) was approximately 4000 M^{-1} cm^{-1}. Since it may be expected that the monoimine complex would have an absorptivity similar to that of $[Ru^{II}(imsar)]^{2+}$ (ϵ_{max} 4000 M^{-1} cm^{-1}),[33] it was reasonable to assume that at this point $[Ru^{II}(imtame)(tame)]^{2+}$ had formed. The ϵ_{max} value of 4000 M^{-1} cm^{-1} also gave a clear indication that oxidation to higher imines (i.e., di, tri, etc.) had not yet taken place. This was consistent with the evidence of the NMR experiment. The same behavior was observed when the OH^- concentration was increased by a factor of 10. Thus the final product had formed to the same extent in the same time, essentially independently of the hydroxide ion concentration.

To observe the first few seconds of the reaction, the experiment was repeated in a stopped-flow spectrophotometer. Absorbance−time profiles were recorded at 390 and 430 nm (Figure S1, Supporting Information). At 430 nm, after an initial growth in absorbance for ~1 s (which could be attributed to the formation of $[Ru^{IV}(tame)_2\text{-}2H^+]^{2+}$) , the absorbance began to decrease, whereas at 390 nm there was a continuous increase in absorbance for approximately 100 s. The traces did not fit either first- or second-order kinetics. When the concentration of the base was increased by a factor of approximately 10, there was no significant change in the shape of these traces. However, when two traces with different $[Ru^{III}(tame)_2]^{3+}$ concentrations were compared at 430 nm, it was clear that there was a difference. For the more dilute solution of $[Ru^{III}(tame)_2]^{3+}$, the growth of the trace at 430 nm continued for a longer time than in the more concentrated solution. This change is significant and shows that there is a dependence of this reaction on the concentration of $[Ru^{III}(tame)_2]^{3+}$. Therefore, a first-order dependence of the reaction can be ruled out. If the $[Ru^{III}(tame)_2]^{3+}$ ion could be deprotonated in this pH range, it would be expected to disproportionate to $[Ru^{II}(tame)_2]^{2+}$ and $[Ru^{IV}(tame)_2\text{-}2H^+]^{2+}$. The $[Ru^{IV}(tame)_2\text{-}2H^+]^{2+}$ could then undergo an intramolecular two-electron redox reaction to form $[Ru^{II}(imtame)(tame)]^{2+}$ at a rate similar to that of the disproportionation. Such a mechanism could account for the lack of isosbestic points in Figure 3 and for the kinetic traces which do not fit either first- or second-order kinetics when the rates of the two processes are comparable.

Increasing the concentration of $[Ru^{III}(tame)_2]^{3+}$ did not increase the rate of the disproportionation reaction to a stage where it could be clearly separated from the imine formation. No matter how fast the initial disproportionation was, it always influenced the trace for the intramolecular conversion of $[Ru^{IV}(tame)_2\text{-}2H^+]^{2+}$ to $[Ru^{II}(imtame)(tame)]^{2+}$. This interference of the disproportionation reaction is evident from the continuous increase in the tail of the trace at 390 nm. Simply, the second-order disproportionation becomes progressively slower and extends over a longer time frame than the first-order reaction. This is very different from the $[Ru^{III}(sar)]^{3+}$ reaction,[33] where the disproportionation rate was much faster than the imine formation rate and the two reactions were well resolved.

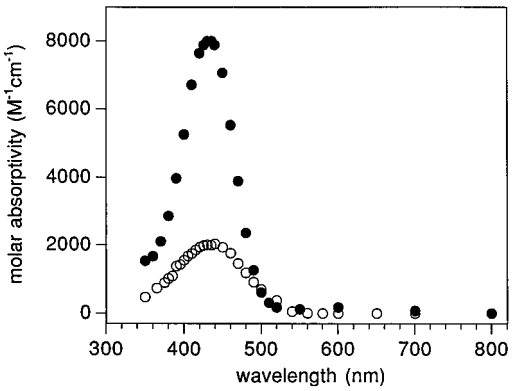

Figure 4. Absorption spectra of $[Ru^{III}(tame)_2\text{-}H^+]^{2+}$ (○) and $[Ru^{IV}(tame)_2\text{-}2H^+]^{2+}$ (●) (25.0 °C, $I = 0.1$ M).

Characterization of $[Ru^{III}(tame)_2\text{-}H^+]^{2+}$. The initial absorbance (at ~1 ms) of the stopped-flow traces (Figure S1) indicated that a new species had been formed within the dead time of the instrument. An obvious candidate for this species is the deprotonated ion $[Ru^{III}(tame)_2\text{-}H^+]^{2+}$. To confirm this, a series of experiments was carried out with the stopped-flow spectrophotometer to measure absorbance as a function of wavelength and time for solutions of $[Ru^{III}(tame)_2]^{3+}$ which had been mixed with NaOH. These traces were recorded for 0.1 s between 350 and 700 nm, and each trace was extrapolated to zero time. The plot of molar absorptivity versus wavelength is shown in Figure 4 (open circles), and this spectrum is attributed to $[Ru^{III}(tame)_2\text{-}H^+]^{2+}$ ($\lambda_{max} = 430$ nm, $\epsilon_{max} = 2000 \pm 50$ M^{-1} cm^{-1}). The ruthenium concentration was varied with no significant change in ϵ_{max}.

The possibility that the spectrum (open circles) in Figure 4 is that of Ru(IV) needs to be addressed. When $[Ru^{IV}(tame)_2\text{-}2H^+]^{2+}$ was generated quantitatively under the same pH conditions using $[Os(CN)_6]^{3-}$ as an oxidant, the peak at 430 nm had $\epsilon_{max} \sim 8000$ M^{-1} cm^{-1}, about 4-fold larger than ϵ_{max} for the putative $[Ru^{III}(tame)_2\text{-}H^+]^{2+}$. Furthermore, the spectral changes described earlier indicated that the disproportionation was taking place in seconds under these conditions, which was too slow to account for the change observed within ~1 ms of addition of OH^-. This conclusion was confirmed by the following experiment. Using a small stopped-flow injector in a nitrogen-filled glovebag, a solution of $[Ru^{III}(tame)_2]^{3+}$ was mixed with OH^- and quenched immediately (≤1 s) by mixing with 3 M HCl. The spectrum of the quenched reaction was that of $[Ru^{III}(tame)_2]^{3+}$ (>95%). When the reaction was quenched at later times, smaller amounts of $[Ru^{III}(tame)_2]^{3+}$ and increasing amounts of $[Ru^{II}(imtame)(tame)]^{2+}$ were observed. These experiments show that the first step in the overall reaction under these conditions is rapid deprotonation of $[Ru^{III}(tame)_2]^{3+}$ and that the spectrum shown in Figure 4 is unequivocally that of $[Ru^{III}(tame)_2\text{-}H^+]^{2+}$.

Acidity Constant of $[Ru^{III}(tame)_2]^{3+}$. A series of experiments was performed in which the initial absorbance at 430 nm, the established λ_{max} of $[Ru^{III}(tame)_2\text{-}H^+]^{2+}$, was measured as a function of pH. The measurement was performed in the same way as for the characterization of $[Ru^{III}(tame)_2\text{-}H^+]^{2+}$.

Apart from deprotonation, virtually no further reaction occurred in 5 ms. According to a standard method,[36] the pK_a was determined as 10.3 ± 0.1 (I = 0.1 M, 25.0 °C).

Characterization of $[Ru^{IV}(tame)_2\text{-}2H^+]^{2+}$. On the basis of the evidence presented so far, the ligand oxidation of $[Ru^{III}(tame)_2]^{3+}$ to $[Ru^{II}(imtame)(tame)]^{2+}$ is arguably proceeding through the Ru(IV) intermediate $[Ru^{IV}(tame)_2\text{-}2H^+]^{2+}$. By analogy with the Ru−sar experiments,[33] at pH ∼11 the doubly-deprotonated species is present rather than the singly-deprotonated form. Since the pK_a values for $[Ru^{III}(sar)]^{3+}$ and $[Ru^{III}(tame)_2]^{3+}$ are 6.3 and 10.3, respectively, the $[Ru^{IV}(tame)_2\text{-}2H^+]^{2+}$ complex would be expected to be more basic than the corresponding sar complex. The pK_a of $[Ru^{IV}(sar)\text{-}H^+]^{3+}$ is reported to be 3 (±1),[33] so the pK_a of $[Ru^{IV}(tame)_2\text{-}H^+]^{3+}$ could be ∼7−8; therefore at pH ∼11, $[Ru^{IV}(tame)_2\text{-}2H^+]^{2+}$ will be the predominant species, rather than $[Ru^{IV}(tame)_2\text{-}H^+]^{3+}$. The formation of $[Ru^{IV}(tame)_2\text{-}2H^+]^{2+}$ was driven to completion by the use of a strong oxidant ($[Os(CN)_6]^{3-}$) and high base concentration (0.050 M OH^-). Stopped-flow traces were recorded at 5 nm intervals for 0.1 s, and each trace was extrapolated to zero time. Although $[Os(CN)_6]^{4-}$ has absorption maxima at 213 and 195 nm,[45] its contribution to the absorbance above 250 nm is negligible. The point by point spectrum of $[Ru^{IV}(tame)_2\text{-}2H^+]^{2+}$ is shown in Figure 4 (filled circles). The spectral parameters (λ_{max} = 430 nm, ϵ_{max} = 8200 ± 100 M^{-1} cm^{-1}) are similar to those obtained for $[Ru^{IV}(sar)\text{-}2H^+]^{2+}$ (λ_{max} at 430 nm, ϵ_{max} 8000 M^{-1} cm^{-1}).[46]

Rate of Formation of $[Ru^{II}(imtame)(tame)]^{2+}$. In order to characterize the reactions that follow the treatment of $[Ru^{III}(tame)_2]^{3+}$ with base, several oxidants were used to generate $[Ru^{IV}(tame)_2\text{-}2H^+]^{2+}$ quantitatively under essentially the same conditions in the stopped-flow mixing chamber. The subsequent reactions of $[Ru^{IV}(tame)_2\text{-}2H^+]^{2+}$ could then be investigated by use of stopped-flow spectrophotometry. For the $[Fe(CN)_6]^{3-}$ oxidation, the kinetic trace measuring the decay of the Ru(IV) species showed first-order kinetics (Figure S2a, Supporting Information). However the points for the first 0.5 s (of the 10 s trace) were removed from the analysis because these included a component arising from the initial electron transfer between $[Ru^{III}(tame)_2\text{-}H^+]^{2+}$ and $[Fe(CN)_6]^{3-}$. The rate constant for the ligand oxidation of tame to imtame was determined as k_{2im} = 1.1 s^{-1}. With O_2 as oxidant, the initial oxidation process was slower, and the trace (Figure S2b, Supporting Information) was treated as two consecutive first-order reactions, giving k_{2im} = 1.1 s^{-1}. The rate of electron self-exchange for $[Os(CN)_6]^{3-/4-}$ is faster, and the redox potential is more positive than that of $[Fe(CN)_6]^{3-/4-}$,[47] so on both counts $[Os(CN)_6]^{3-}$ is a better oxidant. As expected, therefore, the formation of the Ru(IV) intermediate with this oxidant was complete within the stopped-flow dead time (Figure S2c, Supporting Information). The rate constant for decay of the Ru(IV) species was first order (1.1 s^{-1}) and independent of the initial concentration of reactants, in agreement with the O_2 and $[Fe(CN)_6]^{3-}$ experiments. This consistency of the k_{2im} values obtained from the $[Fe(CN)_6]^{3-}$, $[Os(CN)_6]^{3-}$, and O_2 oxidations highlights the usefulness of these oxidants to study such reactions. Clearly, all three are functioning as innocent outer-sphere one-electron reagents. A summary of the experimental conditions and the rate constants is given in Table S1 (Supporting Information). The data show that the rate constant is independent of the concentration and nature of the oxidant, of the $[Ru^{III}(tame)_2]^{3+}$ concentration, and also of the hydroxide ion concentration in this high-pH region. All results are consistent with the conclusion that $[Ru^{IV}(tame)_2\text{-}2H^+]^{2+}$ is being generated quantitatively and rapidly, and the decay observed in the traces (Figure S2) essentially corresponds to a first-order formation of $[Ru^{II}(imtame)(tame)]^{2+}$ from $[Ru^{IV}(tame)_2\text{-}2H^+]^{2+}$.

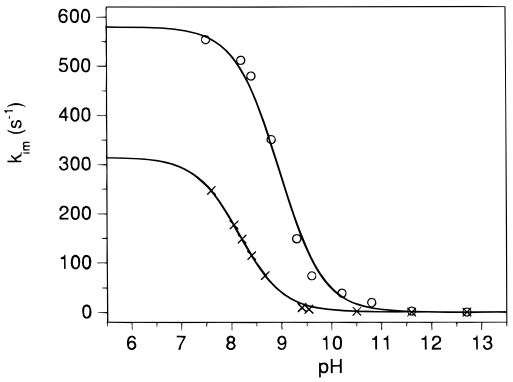

Figure 5. Acid-dependence profile for the formation of $[Ru(imen)(en)_2]^{2+}$ (○) and $[Ru(imtame)(tame)]^{2+}$ (×) from the corresponding deprotonated Ru^{III} complexes (25.0 °C, I = 0.1 M).

The rate of imine formation by intramolecular oxidation of the ligand in the Ru(IV) species was also measured as a function of pH by using $[Os(CN)_6]^{3-}$ as the oxidant (except at pH 12.7 where O_2 was used). The reactions were followed at 390 and 430 nm. At 390 nm, the growth of the imine absorption band followed first-order kinetics and the rates were not significantly different from the first-order decay rate of the band at 430 nm (i.e., the decay of $[Ru^{IV}(tame)_2\text{-}2H^+]^{2+}$). A summary of the experimental conditions and results is given in Table S2 (Supporting Information).

At pH 7.6, a sum of two exponentials was fitted to the data. This allowed the separation of the pseudo-first-order electron-transfer rate constant and the first-order intramolecular redox rate constant. At lower pH, it was difficult to determine the rate constant for the imine formation (k_{im}) as the rate approached the limit of the stopped-flow technique (i.e., $t_{1/2}$ < 0.5 ms). Furthermore, the concentration of $[Ru^{III}(tame)_2\text{-}H^+]^{2+}$ decreased, and the rate of the electron-transfer reaction decreased while the imine formation rate increased. Thus the determination of the rate constant for the imine formation below pH 7 was further complicated by the close overlap of the two rate processes.

The pH dependence of the data (Table S2, Supporting Information) is shown in Figure 5. From this plot it can be seen that the observed rate constant approaches a lower limit at high pH and an upper limit at low pH. The data reflect the existence of two forms of the Ru(IV) intermediate both of which oxidize tame to imtame in the complex. One form, $[Ru^{IV}(tame)_2\text{-}H^+]^{3+}$, is singly deprotonated, while the other, $[Ru^{IV}(tame)_2\text{-}2H^+]^{2+}$, is doubly deprotonated. The pK_a of $[Ru^{III}(tame)_2]^{3+}$ is 10.3, so a pK_a for $[Ru^{IV}(tame)_2\text{-}H^+]^{3+}$ of ∼8 would not be inconsistent with the data in Figure 5 and with corresponding results from the Ru(IV)/Ru(III)−sar system.[33,46,48−50] The reaction sequence for the process is described below:

(45) Sharpe, A. G. *The Chemistry of Cyano Complexes of the Transition Metals*; Academic Press: London, 1976.
(46) Bernhard, P.; Sargeson, A. M.; Anson, F. C. *Inorg. Chem.* **1988**, *27*, 2754.
(47) The value for the $[Os(CN)_6]^{3-/4-}$ self-exchange rate has been determined: k_{11} = 3.2 × 10^4 M^{-1} s^{-1}, I = 0.95 M ($LiClO_4$), 25 °C; $E^{o\prime}$ + 0.69 V, I = 0.5 M (Kläning, U. Department of Chemistry, Aarhus University, Aarhus C, Denmark. Unpublished.
(48) Bernhard, P.; Sargeson, A. M. *J. Chem. Soc., Chem. Commun.* **1985**, 1516.
(49) Bernhard, P.; Sargeson, A. M. *Inorg. Chem.* **1987**, *26*, 4122. The revised electron self-exchange rate constant for $[Ru(sar)]^{3+/2+}$ is 6 × 10^5 M^{-1} s^{-1} at I = 0.2 M.
(50) Bernhard, P.; Anson, F. C. *Inorg. Chem.* **1989**, *28*, 3272.

Intramolecular oxidation of the tame ligand occurs from the two deprotonated forms of the Ru(IV) complex, which account for the limiting rates at high and low pH, respectively.

$$[Ru^{IV}(tame)_2\text{-}H^+]^{3+} \xrightarrow{k_{1im}} [Ru^{II}(imtame)(tame)]^{2+} + H^+$$

$$[Ru^{IV}(tame)_2\text{-}2H^+]^{2+} \xrightarrow{k_{2im}} [Ru^{II}(imtame)(tame)]^{2+}$$

The acid dissociation constant for $[Ru^{IV}(tame)_2\text{-}H^+]^{3+}$ deprotonation is defined by

$$K_{IV} = \frac{[[Ru^{IV}(tame)_2\text{-}2H^+]^{2+}][H^+]}{[[Ru^{IV}(tame)_2\text{-}H^+]^{3+}]}$$

The differential rate law for the decay of the total Ru(IV) concentration is

$$\frac{-d[Ru^{IV}]_t}{dt} = \left(\frac{k_{1im}[H^+] + k_{2im}K_{IV}}{K_{IV} + [H^+]}\right)[Ru^{IV}]_t$$

and the observed rate constant (k_{im}) is

$$k_{im} = \frac{k_{1im}[H^+] + k_{2im}K_{IV}}{K_{IV} + [H^+]} \quad (1)$$

where $[Ru^{IV}]_t$ is the total concentration of Ru(IV) species, k_{1im} is the rate constant for the imine formation from $[Ru^{IV}(tame)_2\text{-}H^+]^{3+}$, and k_{2im} is the rate constant for the imine formation from $[Ru^{IV}(tame)_2\text{-}2H^+]^{2+}$.

A least-squares fit of the data to eq 1 gave the following values: $k_{1im} = 320\ (\pm 20)\ s^{-1}$, $k_{2im} = 1.1\ (\pm 0.3)\ s^{-1}$, $pK_{IV} = 8.2\ (\pm 0.1)$. The oxidation rate constant for the singly deprotonated form is larger than that for the doubly deprotonated form simply because the more highly charged $[Ru^{IV}(tame)_2\text{-}H^+]^{3+}$ is a better oxidant than $[Ru^{IV}(tame)_2\text{-}2H^+]^{2+}$. Similar observations have been made for analogous $[Os^{IV}(en)_3\text{-}H^+]^{3+}$ and $[Os^{IV}(en)_3\text{-}2H^+]^{2+}$ complexes.[24−26] Because it was not possible to collect data at pH <7.6, the value obtained for the limiting rate at low pH ($k_{1im} = 320\ s^{-1}$) is not well defined, but the mechanistic details remain unchanged.

Reevaluation of the Formation of $[Ru^{II}(imsar)]^{2+}$. In the light of this proposed mechanism, the oxidation of the sar complex to $[Ru^{II}(imsar)]^{2+}$ was reviewed. In a previous publication,[33] it was argued that protonation of the metal ion led to imine under acidic conditions. A more likely explanation is that the oxidation occurs from two forms of the Ru(IV) state, i.e. from $[Ru^{IV}(sar)\text{-}H^+]^{3+}$ and $[Ru^{IV}(sar)\text{-}2H^+]^{2+}$. For these complexes, the singly deprotonated form is also expected to be the better oxidant and the rate of imine formation (k_{1im}) is correspondingly faster than that from the doubly deprotonated form (k_{2im}). The data[33] for the sar complex were thus reanalyzed, using the expression for the observed rate constant (k_{im}) as defined in eq 1. The least-squares analysis gave the following values for the sar system: $k_{1im} = 17\ (\pm 1)\ s^{-1}$, $k_{2im} = 5\ (\pm 1) \times 10^{-4}\ s^{-1}$, pK_a(for $[Ru^{IV}(sar)\text{-}H^+]^{3+}$) = 2.0 (±0.1). (Figure 6).

The acid dissociation constant derived from the kinetic data ($pK_a = 2.0 \pm 0.1$) is to be contrasted with that obtained from the electrochemical experiments ($pK_a = 3 \pm 1$).[33] The latter value was derived from a combination of a voltammetric measurement of the $[Ru(sar)]^{3+/2+}$ couple (0.29 V vs NHE in 1.0 M CF_3SO_3H),[48−50] the pH dependence of this couple (in 0.1 M $NaClO_4$), and various kinetic parameters (measured in 0.1 M CF_3SO_3Li).[33] However, an increase of 25 mV in the $[Ru(sar)]^{3+/2+}$ couple on going from 1.0 M CF_3SO_3H to 0.1 M $NaClO_4$ is alone sufficient to account for this difference in pK_a (Table S3 and Figure S3, Supporting Information).

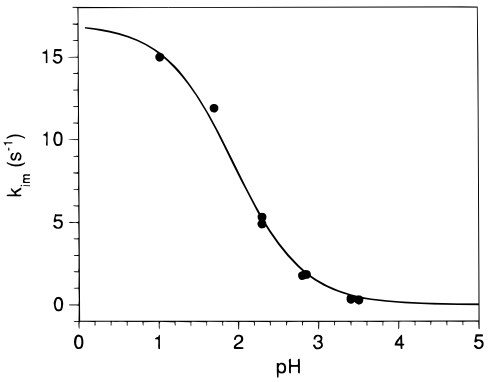

Figure 6. Acid-dependence profile for the formation of $[Ru^{II}(imsar)]^{2+}$ from $[Ru^{IV}(sar)\text{-}H^+]^{3+}$ and $[Ru^{IV}(sar)\text{-}2H^+]^{2+}$ (25.0 °C, $I = 0.1$ M).

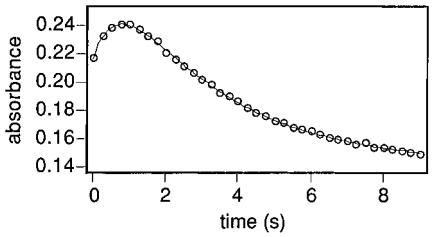

Figure 7. Kinetic traces (experimental data (○) and calculated curve (—) for the reaction of $[Ru^{III}(tame)_2]^{3+}$ (62 μM) in OH^- (4.95 mM) (25.0 °C, $I = 0.1$ M).

Rate of Disproportionation of $[Ru^{III}(tame)_2]^{3+}$. As outlined above, $[Ru^{III}(tame)_2]^{3+}$ disproportionates in basic solutions to $[Ru^{II}(tame)_2]^{2+}$ and $[Ru^{IV}(tame)_2\text{-}2H^+]^{2+}$ and the latter is converted to $[Ru^{II}(imtame)(tame)]^{2+}$. Under the conditions accessible in these experiments, the rate of disproportionation of $[Ru^{III}(tame)_2]^{3+}$ is similar to the rate of imine formation in $[Ru^{IV}(tame)_2\text{-}2H^+]^{2+}$.

To separate these two reactions and obtain their rate constants, it was necessary to deconvolute the kinetic traces using a Runge-Kutta solution (see Experimental Section). Figure 7 shows a simulated trace superimposed on the experimental data for an experiment with $[Ru^{III}(tame)_2]^{3+}$ (62 μM) in OH^- solution (49.5 mM). The parameters used to generate the simulated trace (except for the disproportionation rate constant k_d) were for $[Ru^{III}(tame)_2\text{-}H^+]^{2+}$, $\epsilon_{430} = 2020\ M^{-1}\ cm^{-1}$, for $[Ru^{II}(tame)_2]^{2+}$, $\epsilon_{430} \approx 0$, and for $[Ru^{IV}(tame)_2\text{-}2H^+]^{2+}$, $\epsilon_{430} = 8200\ M^{-1}\ cm^{-1}$; the rate constant for the formation of $[Ru^{II}(imtame)(tame)]^{2+}$ from $[Ru^{IV}(tame)_2\text{-}2H^+]^{2+}$ was taken as $1.1\ s^{-1}$. The rate constants for the disproportionation and comproportionation reactions were varied until a suitable fit was obtained (an example of this procedure is given in Figure S4, Supporting Information). From this analysis the disproportionation rate constant was determined as $3800\ M^{-1}\ s^{-1}$ and the comproportionation rate constant as very much smaller ($<100\ M^{-1}\ s^{-1}$). The simulated trace was insensitive to large variations in the rate constant for comproportionation but very sensitive to minor changes in the rate constant for disproportionation. The disproportionation equilibrium at pH >8 lies very much in favor of the products, consistent with $[Ru^{IV}(tame)_2\text{-}2H^+]^{2+}$ being a weak oxidant unable to oxidize $[Ru^{II}(tame)_2]^{2+}$ to $[Ru^{III}(tame)_2]^{3+}$. The deconvolution process was repeated for kinetic traces of reactions carried out down to pH 9.5. At this pH, the experimental trace was clearly second order for a solution 62 μM in Ru(III), and a second-order rate constant of $1200\ M^{-1}\ s^{-1}$ was derived directly, whereas the deconvoluted fit to this

trace gave the value as 1500 M^{-1} s^{-1}. The similarity of these values implies that the disproportionation reaction no longer has a significant influence on the rate of imine formation. It was independently established that the first-order imine formation rate was considerably faster than the disproportionation rate under the conditions used (Table S2, Supporting Information). Below pH 9.5, it was not necessary to deconvolute the experimental traces to obtain the second-order rate constants because each trace was strictly second order in Ru(III) concentration. A summary of the experimental conditions and kinetic data for the disproportionation reaction, showing both the pH dependence and the dependence on $[Ru^{III}(tame)_2]^{3+}$ concentration, is given in Table S4 (Supporting Information).

Below pH 7, the traces deviated from true second-order kinetics and the rates were not reproducible. Clearly, some other factor was contributing, and attempts to control the reaction in this region by scrupulously removing O_2 and removing traces of extraneous metal ion catalysts with (1,2-ethanediyldinitrilo)-tetraacetate (edta) were unsuccessful. The study was therefore not pursued further in this region. Despite these problems, the data from nearly neutral to strongly basic conditions were reproducible and a meaningful analysis could be made. The data at pH 8.2 at different concentrations of $[Ru^{III}(tame)_2]^{3+}$ (Table S4) illustrate the second-order dependence on Ru(III) concentration. The buffer concentration in all of the above experiments was 0.010 M. A series of experiments in which the buffer concentration was varied (pH 8.23; [buffer] = 0.005, 0.020, 0.100 M; I = 1.0 M) showed no dependence of k_d on the buffer concentration.

If the mechanism for the disproportionation of $[Ru^{III}(tame)_2]^{3+}$ is the same as that proposed for $[Ru^{III}(sar)]^{3+}$ (Scheme 2), then (provided the back-reaction is negligible) the differential rate law for the decay of the Ru(III) would be of the form

$$\frac{-d[Ru^{III}]_t}{dt} = \frac{k_d K_a [H^+][Ru^{III}]_t^2}{(K_a + [H^+])^2}$$

and the observed second-order rate constant would be

$$k_{obs} = \frac{k_d K_a [H^+]}{(K_a + [H^+])^2} \qquad (2)$$

If this rate law were correct, the observed rate constant would be at a maximum when the concentrations of the protonated and deprotonated forms were equal. However, the observed data are not in agreement with this rate law. It is therefore proposed that the limiting rate constant at high pH arises from a disproportionation reaction between two deprotonated molecules of the Ru(III) complex

$$2[Ru^{III}(tame)2\text{-}H^+]^{2+} \xrightarrow{k_{2d}} [Ru^{II}(tame)_2]^{2+} + [Ru^{IV}(tame)_2\text{-}2H^+]^{2+}$$

This equilibrium favors the products, since $[Ru^{IV}(tame)_2\text{-}2H^+]^{2+}$ is not a sufficiently strong oxidant to oxidize $[Ru^{II}(tame)_2]^{2+}$ to $[Ru^{III}(tame)_2]^{3+}$. Keene et al.[15−17] speculated that a disproportionation process was possible between two singly deprotonated Ru(III)−amine complexes, but the lack of a suitable oxidant prevented them from investigating this possibility further. However, to accommodate the rate data overall, both this path and the following path are required:

$$[Ru^{III}(tame)_2\text{-}H^+]^{2+} + [Ru^{III}(tame)_2]^{3+} \xrightarrow{k_{1d}} [Ru^{II}(tame)_2]^{2+} + [Ru^{IV}(tame)_2\text{-}H^+]^{3+}$$

The proposed model for the overall process is given in Scheme 3, and provided the back-reactions are negligible, the overall differential rate law is

$$\frac{-d[Ru^{III}]_t}{dt} = \frac{(k_{1d}K_a[H^+] + k_{2d}K_a^2)[Ru^{III}]_t^2}{(K_a + [H^+])^2}$$

and the observed second-order rate constant k_d is given by

$$k_d = \frac{(k_{1d}K_a[H^+] + k_{2d}K_a^2)}{(K_a + [H^+])^2} \qquad (3)$$

At $[H^+] \ll K_a$, k_d equals k_{2d}, which accounts for the high-pH limit. A least-squares fit to the observed rate constants using eq 3 and a value of K_a determined by the spectrophotometric titration ($pK_a = 10.3 \pm 0.1$) is shown in Figure 8, giving values of $k_{1d} = 8300$ (±1000) M^{-1} s^{-1} and $k_{2d} = 3900$ (±100) M^{-1} s^{-1}. The result that $k_{1d} > k_{2d}$ seems reasonable because $[Ru^{III}(tame)_2]^{3+}$ is a better oxidant than $[Ru^{III}(tame)_2\text{-}H^+]^{2+}$.

As the pH decreases however, the comproportionation reaction must become significant and the rate law given above amended. It was not possible to control the reaction in this region, as described earlier, but clearly the limiting condition at low pH required by the simplified rate law would only be realized approximately and that is evident from the low-pH region of Figure 8.

Reactions of $[Ru^{III}(en)_3]^{3+}$. It has long been known that basic solutions of $[Ru^{II}(en)_3]^{2+}$ and $[Ru^{III}(en)_3]^{3+}$ produce the yellow $[Ru^{II}(diimen)(en)_2]^{2+}$ complex (λ_{max} = 448 nm, ϵ_{max} = 6900 M^{-1} cm^{-1}) when exposed to air.[10,12,44] Partial oxidation of $[Ru^{III}(en)_3]^{3+}$ (presumably to a monoimine species) also occurs in the absence of air, and this reaction has now been examined in more detail. The reaction was followed spectrophotometrically, taking the necessary precautions to prevent oxidation by adventitious O_2. A solution of $[Ru^{III}(en)_3]^{3+}$ was mixed with a NaOH solution ($[OH^-]$ = 0.045 M), and the spectrum of the reaction mixture was recorded every 5 s. The spectra for the first 20 s are shown in Figure 9a. The band which initially appears at 420 nm (trace a) decays in the first 5 s, and a new band appears at 370 nm (trace b). This band has been attributed to formation of the monoimine. When this sample is exposed to air, the band at 370 nm decays, and a new band of approximately twice the intensity appears at 448 nm (Figure 9b). The isosbestic point and intensity changes for the second reaction imply conversion of the monoimine to the diimine without a significant build-up of an intermediate.

Upon further examination of the monoimine formation, it is clear that the reactivity of $[Ru^{III}(en)_3]^{3+}$ is very similar to that of $[Ru^{III}(tame)_2]^{3+}$. The characterization of $[Ru^{III}(en)_3\text{-}H^+]^{2+}$ and $[Ru^{IV}(en)_3\text{-}2H^+]^{2+}$ and the determination of the acidity constant of $[Ru^{III}(en)_3]^{3+}$ followed the same procedure as that used for $[Ru^{III}(tame)_2]^{3+}$. $[Ru^{III}(en)_3\text{-}H^+]^{2+}$ has its λ_{max} at 430 nm with $\epsilon_{max} = 3100 \pm 100$ M^{-1} cm^{-1} (I = 0.10 M, 25.0 °C). By analogy with the $[Ru^{III}(tame)_2\text{-}H^+]^{2+}$ system, interference with the measurement of the pK_a of $[Ru^{III}(en)_3]^{3+}$ from the disproportionation reaction was negligible on the millisecond time scale. The pK_a was determined as 10.4 ± 0.1 (I = 0.10 M, 25.0 °C), very similar to the value found for the $[Ru^{III}(tame)_2]^{3+}$ ion (pK_a = 10.3) and much higher than that for $[Ru^{III}(sar)]^{3+}$ (pK_a = 6.3).[46] The molar absorption coefficient for $[Ru^{IV}(en)_3\text{-}2H^+]^{2+}$ was determined as 4100 ± 100 M^{-1} cm^{-1}

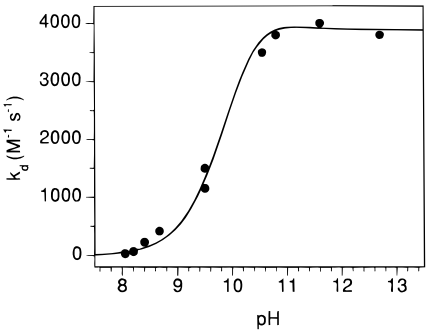

Figure 8. Acid-dependence profile of the second-order rate constants (k_d) for the disproportionation reactions of $[Ru^{III}(tame)_2]^{3+}$ (25.0 °C, I = 0.1 M).

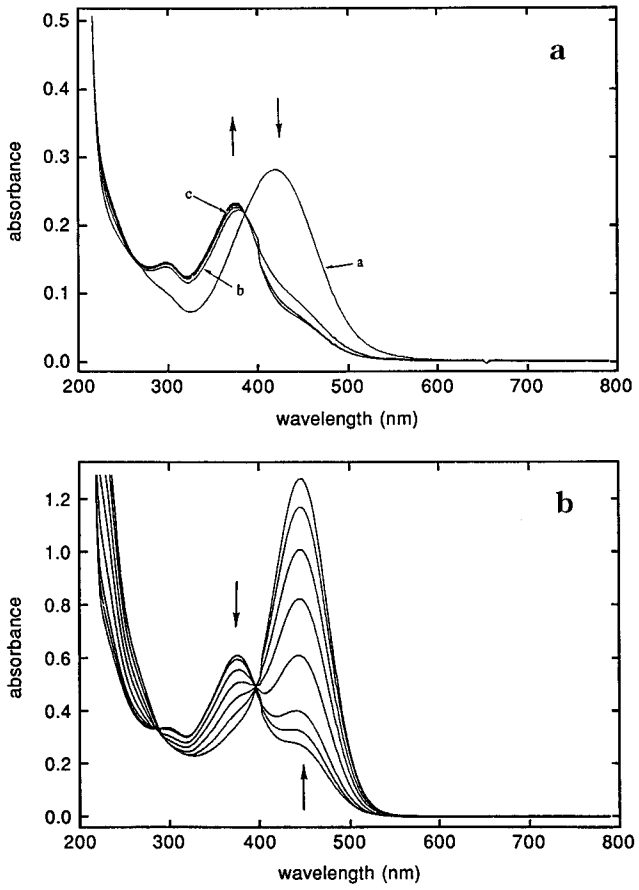

Figure 9. (a) Absorption spectra of a reaction mixture containing $[Ru^{III}(en)_3]^{3+}$ (129 μM) in OH^- solution (4.5 mM) recorded at 5 s intervals. (b) Absorption spectra for the oxidation of $[Ru^{II}(imen)(en)_2]^{2+}$ to $[Ru^{II}(diim)(en)_2]^{2+}$ recorded at 5 min intervals after complete conversion of $[Ru^{III}(en)_3]^{3+}$ (381 μM) to $[Ru^{II}(imen)(en)_2]^{2+}$ (25.0 °C, I = 0.1 M).

at the λ_{max} of 420 nm (I = 0.10 M, 25.0 °C), approximately half that obtained for the $[Ru^{IV}(tame)_2\text{-}2H^+]^{2+}$ and $[Ru^{IV}(sar)\text{-}2H^+]^{2+}$ ions.

Rate of Formation of $[Ru^{II}(imen)(en)_2]^{2+}$. In order to eliminate the complications arising from the Ru(III) disproportionation reaction, $[Ru^{IV}(en)_3\text{-}2H^+]^{2+}$ was generated directly and quantitatively in the time of mixing by using $[Os(CN)_6]^{3-}$ as an oxidant.[47] The intramolecular redox reaction of $[Ru^{IV}(en)_3\text{-}2H^+]^{2+}$ to form $[Ru^{II}(imen)(en)_2]^{2+}$ was then readily followed at 420 nm (pH 11.6, 25 °C). The rate of decay of $[Ru^{IV}(en)_3\text{-}2H^+]^{2+}$ was first order with a rate constant of 3.1 (±0.1) s^{-1}.

The imine formation in deprotonated $[Ru^{IV}(en)_3]^{4+}$ was also measured as a function of pH. $[Os(CN)_6]^{3-}$ was used as the oxidant as before, and this reaction was followed at 420 nm where the decay of [Ru(IV)] was first order. The experimental conditions and results are summarized in Table S5 (Supporting Information) . These results are similar to those obtained for the oxidation of $[Ru^{IV}(tame)_2\text{-}2H^+]^{2+}$ and $[Ru^{IV}(tame)_2\text{-}H^+]^{3+}$ and have been interpreted in the same manner as shown below:

Intramolecular oxidation of the en ligand occurs from two deprotonated forms of the Ru(IV) complex which account for the limiting rates at high and low pH, respectively.

$$[Ru^{IV}(en)_3\text{-}H^+]^{3+} \xrightarrow{k_{1im}} [Ru^{II}(imen)(en)_2]^{2+} + H^+$$

$$[Ru^{IV}(en)_3\text{-}2H^+]^{2+} \xrightarrow{k_{2im}} [Ru^{II}(imen)(en)_2]^{2+}$$

The acid dissociation constant for $[Ru^{IV}(en)_3\text{-}H^+]^{3+}$ deprotonation is defined by

$$K_{IV} = \frac{[[Ru^{IV}(en)_3\text{-}2H^+]^{2+}][H^+]}{[[Ru^{IV}(en)_3\text{-}H^+]^{3+}]}$$

This leads to the same differential rate law for the decay of the total Ru(IV) concentration as that derived above for the bis-tame ruthenium system. From a least-squares fit of the data in Table S5 to eq 1, the following values were obtained: k_{1im} = 600 (±20) s^{-1}, k_{2im} = 1.0 (±0.4) s^{-1}, pK_{IV} = 8.9 (±0.1). The pH profile is shown in Figure 5 along with the corresponding profile for the bis-tame ruthenium system. Even on a quantitative basis, these two systems behave in remarkably similar manners.

Rate of Disproportionation of $[Ru^{III}(en)_3]^{3+}$. Because of the reactivity patterns of $[Ru^{III}(sar)]^{3+}$ and $[Ru^{III}(tame)_2]^{3+}$ in basic solutions, it was expected that $[Ru^{III}(en)_3]^{3+}$ would also disproportionate to $[Ru^{II}(en)_3]^{2+}$ and $[Ru^{IV}(en)_3\text{-}2H^+]^{2+}$ and that the latter would proceed to the imine. It is clear from the data that the monoimine complex forms after disproportionation of the Ru(III) species and the rate of disproportionation of $[Ru^{III}(en)_3\text{-}H^+]^{2+}$ is comparable with the rate of imine formation from $[Ru^{IV}(en)_3\text{-}2H^+]^{2+}$. To obtain the rate constants of these two reactions separately, it was necessary to deconvolute the rate traces using a Runge-Kutta solution by analogy with the $[Ru^{III}(tame)_2]^{3+}$ system in base. According to the method outlined above, the value determined for the disproportionation rate constant was 4000 M^{-1} s^{-1}. In this case also, the simulated trace was insensitive to large variations in the rate of comproportionation but very sensitive to minor changes in the rate of disproportionation, so it would seem that the uncertainty for the disproportionation rate constant is not large. As for the reaction of $[Ru^{III}(tame)_2]^{3+}$, the disproportionation equilibrium lies very much in favor of the products. When this reaction was followed at pH 8.99, the trace obeyed strictly second-order kinetics, and a second order rate constant of 405 M^{-1} s^{-1} was obtained. It was not necessary to deconvolute the traces in the region where the pH was significantly below the pK_a of $[Ru^{III}(en)_3]^{3+}$. A summary of the values for the rate constant of the disproportionation reaction is given in Table S6 (Supporting Information). The proposed mechanism for this reaction is the same as that for $[Ru^{III}(tame)_2]^{3+}$ (Scheme 3).

A least-squares fit of the data in Table S6 to the rate law derived for this mechanism and the value for K_a determined by the spectrophotometric titration (pK_a = 10.4 ± 0.1) gives the values k_{1d} = 9000 (±2000) M^{-1} s^{-1} and k_{2d} = 3800 (±350) M^{-1} s^{-1}. The fit of the data to the rate law with these parameters is shown in Figure S5 (Supporting Information). The values of pK_a, k_{1d}, and k_{2d} are very similar to the values for the analogous ruthenium tame complexes but very different from those of the ruthenium sar system.

Table 1. Properties of Ru(II) and Ru(III) Complexes in Aqueous Solution at 25 °C

complex	λ_{max} (ϵ_{max}), nm (M^{-1} cm^{-1})	k_{11},[a] M^{-1} s^{-1}	E'(III/II), V (vs NHE)	pK_a	k_{1d}, M^{-1} s^{-1}	k_{2d}, M^{-1} s^{-1}
$[Ru^{II}(sar)]^{2+}$ [b]	385 (40)	6×10^5		≫15		
	282 (2000)					
$[Ru^{III}(sar)]^{3+}$ [b]	reacts too fast to measure		0.290	6.3[c]	$(6-9) \times 10^7$	$>10^7$
					4×10^7 [d]	$\geq 2 \times 10^7$ [d]
$[Ru^{II}(tame)_2]^{2+}$	380 (70)	3.5×10^4 [e]		≫15		
	285 (1090)					
$[Ru^{III}(tame)_2]^{3+}$	352 (459)		0.03	10.3	8300	
$[Ru^{III}(tame)_2\text{-}H^+]^{2+}$	430 (2000)			>15		3900
$[Ru^{II}(en)_3]^{2+}$ [f]	370 (40[d])	3.1×10^4 [g]		≫15		
	302 (1020)					
$[Ru^{III}(en)_3]^{3+}$ [f]	310 (360)		0.15[h]	10.4	9000	
$[Ru^{III}(en)_3\text{-}H^+]^{2+}$	430 (3100)			>15		3800
$[Ru^{II}(NH_3)_6]^{2+}$ [f]	390 (35)	3×10^3 [i]		≫15		
	275 (640)					
$[Ru^{III}(NH_3)_6]^{3+}$ [f]	320 (100)		0.07[h]	12.4[j]		
	275 (480)					
$[Ru^{II}(capten)]^{2+}$ [k,l]	338 (670)		1.18	≫15		
	250 (3880)					
$[Ru^{II}(tacn)_2]^{2+}$ [h,m]	355 (60)	5×10^4		≫15		
	267 (980)					
$[Ru^{III}(tacn)_2]^{3+}$ [h,m]	375 (330)		0.37			

[a] Self exchange rate constant for Ru(III)/Ru(II) electron transfer. [b] Reference 33 and 48−50. [c] Reference 46. [d] This work. [e] Reference 41. [f] Electronic spectra from refs 42 and 53. [g] Reference 54. [h] Reference 53. [i] Reference 55. [j] Reference 56. [k] capten = 1-methyl-3,13,16-trithia-6,10,19-triazabicyclo[6.6.6]icosane. [l] Reference 57. [m] tacn = 1,4,7-triazacyclononane.

Table 2. Properties of Ru(IV) Complexes in Aqueous Solution at 25 °C

complex ion	λ_{max} (ϵ_{max}), nm (M^{-1} cm^{-1})	pK_a	k_{1im}, s^{-1}	k_{2im} s^{-1}
$[Ru^{IV}(sar)\text{-}H^+]^{3+}$	445 (7800)[a]	2.0 ± 0.1[b]	17	
		2.9 ± 1.3[c]		
$[Ru^{IV}(sar)\text{-}2H^+]^{2+}$	430 (8000)[d]	>15		5×10^{-4}
$[Ru^{IV}(tame)_2\text{-}H^+]^{3+}$		8.2 ± 0.1	320	
$[Ru^{IV}(tame)_2\text{-}2H^+]^{2+}$	430 (8200)	>15		1.1
$[Ru^{IV}(en)_3\text{-}H^+]^{3+}$		8.9 ± 0.1	600	
$[Ru^{IV}(en)_3\text{-}2H^+]^{2+}$	420 (4100)	>15		1.0
$[Ru^{IV}(tacn)_2\text{-}H^+]^{3+}$	not stabilized like those above			

[a] Reference 33. [b] This work; derived from solution kinetics ($I = 0.1$ M ($NaClO_4$)). [c] Derived from voltammetric studies ($I = 1.0$ M (CF_3SO_3H)); reference 50. The value was miscalculated (3.0 ± 0.6) in the original reference). [d] Reference 46.

Discussion

The complex ions $[Ru^{III}(tame)_2]^{3+}$ and $[Ru^{III}(en)_3]^{3+}$ were examined because they can be considered as representative substructures of the cage complex $[Ru^{III}(sar)]^{3+}$. They were chosen to test the influence of the ligand structure on intramolecular imine formation and to see if one complex or the other could account for the unusually rapid amine oxidation in the $[Ru^{III}(sar)]^{3+}$ ion.

The ligand dehydrogenation reactions of the three systems are quite complex, but their mechanisms are similar; they correspond to that given in Scheme 3. The overall rates can be influenced by a number of factors. It is instructive therefore to look at the situation in some detail.

A summary of the results, Tables 1 and 2, shows that the overall reactivity of $[Ru^{III}(en)_3]^{3+}$ is quite similar to that of $[Ru^{III}(tame)_2]^{3+}$. The Ru(III)/Ru(II) electron self-exchange rate constants are similar in magnitude;[41] the pK_a values for Ru(III) are the same within experimental error; the rates of disproportionation are much the same despite the variation in their (III)/(II) redox potentials; the disproportionation equilibria for both complexes in basic solution lie very much in favor of the Ru(II) and Ru(IV) products; the pK_a's for the mono-deprotonated Ru(IV) complexes are similar, and the imine formation rate constants k_{1im} and k_{2im} are also similar, respectively. If the difference of 0.12 V between the redox couples $[Ru(en)_3]^{3+/2+}$ and $[Ru(tame)]^{3+/2+}$ were the sole influence on the rates of disproportionation, then there should have been maximally a 100-fold difference in the rates of disproportionation. Since the rates are similar, some other factor must counterbalance this difference. Moreover, since the rates of the disproportionation reactions are so similar, there is no kinetic property inherent in either the en or the tame complex which accounts for the rapid reaction of $[Ru^{III}(sar)]^{3+}$.

An analogous comparison of the rates of imine formation indicates that there is no property inherent in these complexes which accounts for the regiospecific formation of the imine in the cap of the $[Ru^{III}(sar)]^{3+}$ complex. However, some features have been observed which help explain the overall reactivity difference between $[Ru^{III}(tame)]^{3+}$ and $[Ru^{III}(en)_3]^{3+}$ versus the $[Ru^{III}(sar)]^{3+}$ complex under the different pH conditions.

The disproportionation reaction only proceeds once the Ru(III) ion is deprotonated, and there are substantial differences in the acidities of the M(III) species. $[Ru^{III}(sar)]^{3+}$ (p$K_a = 6.3$) is much more acidic than either $[Ru^{III}(tame)_2]^{3+}$ (p$K_a = 10.3$) or $[Ru^{III}(en)_3]^{3+}$ (p$K_a = 10.4$). The lower pK_a is attributed to strain in the hexadentate ligand which is relieved somewhat when $[Ru^{III}(sar)]^{3+}$ is deprotonated. This strain is also evident in the fast electron self-exchange for $[Ru(sar)]^{3+/2+}$ ($k_{11} = 6 \times 10^5$ M^{-1} s^{-1} at 25 °C),[49] which we have attributed to the virtually identical coordination geometries of the $[Ru^{II}(sar)]^{2+}$ and $[Ru^{III}(sar)]^{3+}$ cations, engendered by the cage structure of the sar ligand.[51] The difference in the K_a values makes the deprotonated $[Ru^{III}(sar)]^{3+}$ species ~10^4-fold more accessible at lower pH than either of the other deprotonated complexes.

Not only is the deprotonated substrate of $[Ru^{III}(sar)]^{3+}$ more accessible by 4 orders of magnitude but the disproportionation rate constant is also 4 orders of magnitude larger than the corresponding rate constants for $[Ru^{III}(en)_3]^{3+}$ and $[Ru^{III}(tame)_2]^{3+}$. The disproportionated products are therefore more favored for $[Ru^{III}(sar)]^{3+}$ than for the other two complexes. $[Ru^{II}(sar)]^{2+}$ is also a favored product because the (III)/(II) reduction

(51) Bernhard, P.; Bürgi, H. B.; Raselli, A.; Sargeson, A. M. *Inorg. Chem.* **1989**, *28*, 3234.

Scheme 4

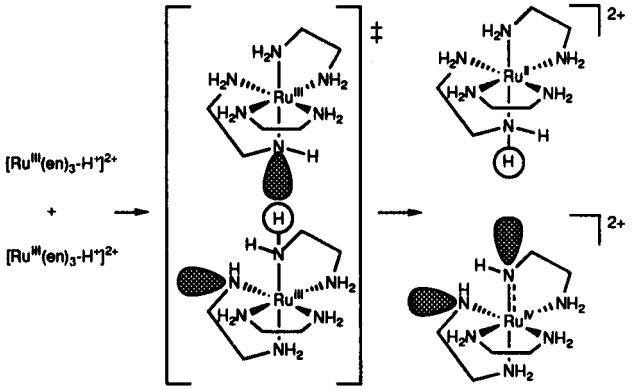

Scheme 4a

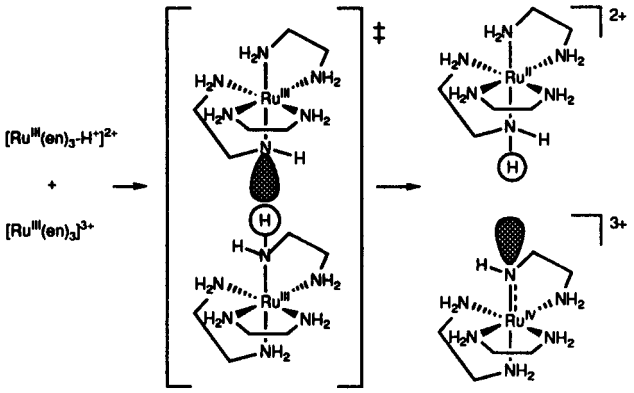

Scheme 4b

potential is more positive than those of the other two molecules, and the formation of the Ru(IV) state is favored by the stabilization which arises from the loss of two protons. The very low pK_a for $[Ru^{IV}(sar)\text{-}H^+]^{3+}$ means that the doubly deprotonated form is at least 5 orders of magnitude more accessible than the corresponding forms of the complexes of the two cage fragments. So, both kinetically and thermodynamically, the disproportionation of $[Ru^{III}(sar)]^{3+}$ is favored over the disproportionation of $[Ru^{III}(en)_3]^{3+}$ and $[Ru^{III}(tame)_2]^{3+}$.

The structural requirements of the two possible disproportionation reactions of the Ru(III) complexes are quite different. They are discussed below in detail for the en system, but the same arguments apply for the tame and sar systems. For the path involving a deprotonated $[Ru^{III}(en)_3\text{-}H^+]^{2+}$ and fully protonated $[Ru^{III}(en)_3]^{3+}$ ion, it is obvious to invoke simple outer-sphere electron transfer with the deprotonated Ru(III) complex acting as the reductant. This would leave the Ru(II) product fully protonated and the Ru(IV) product singly deprotonated. Reaction between two deprotonated $[Ru^{III}(en)_3\text{-}H^+]^{2+}$ ions however requires a coupled e^- and H^+ transfer, (i.e., a net hydrogen atom transfer), presumably with an activated complex involving a hydrogen bond between the two complexes (Scheme 4a). A concerted path is necessary because a deprotonated Ru(II) complex is not a feasible intermediate product. Simply, it is difficult and slow to deprotonate these Ru(II)−amine complexes because their pK_a values are much in excess of 15. The transfer could however be conducted through a water bridge. If the structures of the $[Os^{IV}(en)(en\text{-}H)_2]^{2+}$ and $[Os^{IV}(tmen)(tmen\text{-}H)_2]^{2+}$ complex cations[25,52] are a guide to the Ru(IV) structures, it is unlikely that one ethanediamine fragment will be doubly deprotonated; rather, the deprotonations will be *cis* to each other on different en residues. For the tame and sar complexes, it is more difficult to gauge the regiospecificity of the two deprotonation sites.

An alternative view of the disproportionation mechanism is tenable if the similarity of the rates of both the tame and en complexes (k_{1d} and k_{2d}) is considered significant. Such agreement might arise from very similar H atom transfer paths for both reactions, irrespective of the degree of deprotonation of the reaction partners. In this case, the reaction between $[Ru^{III}(en)_3\text{-}H^+]^{2+}$ and $[Ru^{III}(en)_3]^{3+}$ also involves an atom transfer reaction (Scheme 4b). It is not possible to distinguish between the two possibilities for the disproportionation reaction involving $[Ru^{III}(en)_3]^{3+}$ and $[Ru^{III}(en)_3\text{-}H^+]^{2+}$ on the basis of the experimental results, but a study in D_2O could possibly throw some light on the issue if N−H bond breaking were a significant component.

The rate of imine formation for the Ru(IV) state is significantly dependent on the ligand and whether it is singly or doubly deprotonated. For all these systems, intramolecular ligand oxidation occurs more rapidly in the singly deprotonated form of the Ru(IV) complex than in the doubly deprotonated form. This is not surprising considering that the reduction potential of the Ru(IV/III) couple is expected to be more positive for the singly deprotonated form. However, under both conditions, the intramolecular oxidations of both tame and en ligands occur more rapidly than that of the sar ligand. This is attributed to the lesser strain involved in the formation of the imine product with the more flexible ligands than with the cage. For the $[Ru^{II}(sar)]^{2+}$ and $[Ru^{III}(sar)]^{3+}$ complexes, there is an inherent strain caused by the steric demands of the encapsulating ligand; this can be relieved in part by forming the delocalized Ru^{IV}═N ion, but it is not relieved in forming $[Ru^{II}(imsar)]^{2+}$. That can be seen more clearly when the oxidation progresses to the hexaimine and the strain increases drastically, distorting the molecule.[41] It is twisted along the C_3 axis 31° toward a trigonal prismatic orientation of the six ligating atoms. Overall, therefore, the $[Ru^{III}(sar)]^{3+}$ ion dehydrogenates more readily at pH <7 largely because of the favorable disproportionation rates and equilibria compared with the case of $[Ru^{III}(en)_3]^{3+}$ and $[Ru^{III}(tame)_2]^{3+}$. In much more basic solution, the reverse is the case, simply because the intramolecular redox reaction is faster ($\sim 10^3$-fold) for the simpler complexes than for the cage complex.

These reactions are obviously very complex and are clearly governed by the acidities, ligand strain, and disproportionation rates of the M(III) state, the inherent rate of oxidation of the M(IV) state, the strain and orientation factors which stabilize or destabilize the delocalized M(IV) state, and whether or not the M(IV) state is doubly or singly deprotonated. The stability of the M(II) imine may also influence the final step. These final steps will be examined more closely in a subsequent publication which also addresses the regiospecificity of $[Fe^{IV}(sar)]$ oxidation paths. The identification and elaboration of these factors and their magnitude should allow an intimate understanding of such M(IV) → M(II) intramolecular oxidations and should contribute to the design of efficient catalysts for intramolecular $2e^-$ oxidations in instances where the substrate can bind to the metal center.

(52) Patel, A.; Ludi, A.; Bürgi, H. B.; Raselli, A.; Bigler, P. *Inorg. Chem.* **1992**, *31*, 3405.
(53) Bernhard, P.; Sargeson, A. M. *Inorg. Chem.* **1988**, *27*, 2582.
(54) Beattie, J. K.; Smolenaers, P. J. *J. Phys. Chem.* **1986**, *90*, 3684.
(55) Brown, G. M.; Sutin, N. *J. Am. Chem. Soc.* **1979**, *101*, 883.
(56) Waysbort, D.; Navon, G. *J. Chem. Soc., Chem. Commun.* **1971**, 1410.
(57) Bernhard, P.; Bull, D. J.; Robinson, W. T.; Sargeson, A. M. *Aust. J. Chem.* **1992**, *45*, 1241.

Acknowledgment. The assistance of the ANU Microanalytical Unit is gratefully acknowledged, and the authors are grateful to Professor D. J. Evans for writing the kinetics program based on a Runge-Kutta solution.

Supporting Information Available: Details of the program REACTION KINETICS used to deconvolute kinetic traces and examples of the fitting (Figure S4); assignment of the NMR spectra for $[Ru^{II}(imtame)(tame)]^{2+}$; absorbance−time profiles of $[Ru^{III}(tame)_2]^{3+}$ mixed with base (Figure S1); absorbance−time profiles (and lines of best fit) of $[Ru^{III}(tame)_2]^{3+}$ mixed with base and various oxidants (Figure S2); kinetic data for the formation of $[Ru^{II}(imtame)(tame)_2]^{2+}$ from $[Ru^{IV}(tame)_2\text{-}H^+]^{3+}$ and $[Ru^{IV}(tame)_2\text{-}2H^+]^{2+}$ (Tables S1 and S2); calculations showing the effect of variations in $E_{III/II}$ on pK_{IV} for the [Ru(sar)] system (Table S3); acid-dependence data for the formation of $[Ru^{II}(imsar)]^{2+}$ fitted to the rate expression with various values of pK_{IV} (Figure S3); kinetic data for the disproportionation of $[Ru^{III}(tame)_2]^{3+}$ (Table S4); kinetic data for the formation of $[Ru^{II}(imen)(en)_2]^{2+}$ from $[Ru^{IV}(en)_3\text{-}H^+]^{3+}$ and $[Ru^{IV}(en)_3\text{-}2H^+]^{2+}$ (Table S5); kinetic data for the disproportionation of $[Ru^{III}(en)_3]^{3+}$ (Table S6); pH dependence profile of the second-order rate constants (k_d) for the disproportionation of $[Ru^{III}(en)_3]^{3+}$ (Figure S5) (17 pages). Ordering information is given on any current masthead page.

IC961021Q